

Synthesis and Self-Assembly of Novel Amphiphilic Copolymers Poly(lactic acid)-*block*-Poly(ascorbyl acrylate)

Yanzhai Wang,¹ Junjiao Yang,² Jing Yang¹

¹State Key Laboratory of Chemical Resource, College of Life Science and Technology, Beijing University of Chemical Technology, Beijing 100029, China

²College of Science, Beijing University of Chemical Technology, Beijing 100029, China

Correspondence to: J. Yang (E-mail: yangjingbuct@gmail.com)

Received 24 May 2011; accepted 17 June 2011; published online 7 July 2011

DOI: 10.1002/pola.24840

ABSTRACT: In this study, a novel type of amphiphilic block copolymers poly(lactic acid)-*block*-poly(ascorbyl acrylate) (PLA-*block*-PAAA) with biodegradable poly(lactic acid) as hydrophobic block and poly(ascorbyl acrylate) (PAAA) as hydrophilic block was successfully developed by a combination of ring-opening polymerization and atom transfer radical polymerization, followed by hydrogenation under normal pressure. The chemical structures of the desired copolymers were characterized by ¹H NMR and gel permeation chromatography. The thermal physical properties and crystallinity were investigated by thermogravimetric analysis, differential scanning calorimetry, and wide angle X-ray diffraction, respectively. Their self-assem-

bly behavior was monitored by fluorescence-probe technique and turbidity change using UV-vis spectrometer, and the morphology and size of the nanocarriers via self-assembly were detected by cryo-transmission electron microscopy and dynamic light scattering. These polymeric micelles with PAAA shell extending into the aqueous solution have potential abilities to act as promising nanovehicles for targeting drug delivery. © 2011 Wiley Periodicals, Inc. *J Polym Sci Part A: Polym Chem* 49: 3988–3996, 2011

KEYWORDS: block copolymers; drug delivery system; self-assembly

INTRODUCTION Targeting strategies for drug nanocarriers are currently receiving much attention in nanomedicine due to their unique advantage of improving the effects of drugs against various biological models.^{1,2} Besides their outstanding merits, such as enhancing the bioavailability of drugs in physiological environment and sustaining release of compounds for long-term therapy,³ more importantly, the targetable nanocarriers can play an active role to increase specifically cellular delivery, thereby to reduce harmful effects of the loaded drugs on nontargeted cells.⁴ In recent years, the successful exploitation of various endogenous biomolecules and specific nutrients responsible for tumor tissues and organs has shed light on the development of drug delivery from passive to active targeting.^{5–7} Nanocarriers design combining with a good knowledge of biochemical features difference between normal and tumoral cells would be broadly investigated as an extremely important way to realize active targeting strategy in the field of drug delivery.

Ascorbate (*L*-ascorbic acid, AA) as an essential molecule for man has been recognized for many years. In recent years, a great deal of research has focused on the special physiology of ascorbate. For example, abnormal local accumulation of ascorbate in tumor tissue has been found as a result of ele-

vated levels of superoxide produced by stromal and/or tumor cells.^{8–10} The studies on neuroprotective role of ascorbate and the mechanism of its penetration into the brain presented the molecular selectivity and physiological disposition between ascorbate and sodium-dependent vitamin C transporters SVCT2.^{11,12} These biochemical discoveries exhibited the significance of ascorbate in the treatment of tumors and central nervous disorders, meanwhile, also hinted that it might serve to improve the specificity of overall drug delivery system to the pathological sites if ascorbate as a promising targeting molecule is used to modify drug carriers.

Actually, a few studies are available in the literature on AA as biological target mediating the specific delivery of therapeutic or diagnostic molecules. Manfredini et al. reported that small molecule prodrugs were fabricated by chemical conjugation of AA with central nervous system (CNS) active molecules. It was shown that AA endowed such prodrugs with efficient binding features to epithelial-associated SVCT2 translocator, which benefited to the effective drug release in the vicinity of the site of action.^{13–15} Although a short biological life of such prodrugs in the bloodstream circulation would be one key barrier to enhance the whole therapeutic

Additional Supporting Information may be found in the online version of this article

© 2011 Wiley Periodicals, Inc.

efficiency, these results highlighted the potential of AA transporter as a new mediator for drug delivery. Taking advantage of liposome and ascorbate features, Torchilin's group thoroughly studied the ability of ascorbate-modified liposome to target and kill certain types of tumor cells and to potentiate the effect of the anticancer drugs delivered by these liposomes,^{16–18} which supported that ascorbate-mediated nanocarriers might be particularly effective in targeting cancers. Moreover, this type of liposomes was also investigated in targeting the CNS, and further exhibited their great potential in the application of specific brain delivery.¹⁹ Besides, Durán and coworkers²⁰ reported that the nanoparticles capped by ascorbate via nonconjugated bond showed good antitumoral activity, as well. Among the reported examples, only one AA was bonded at one end of the molecular architecture for conducting its targeting property and adjusting the whole molecular hydrophilic/hydrophobic balance. To the best of our knowledge, few have been reported on the amphiphilic polymers with polymeric AA as hydrophilic block.

Inspired by particular biological properties of AA, we synthesize a class of block copolymers with biodegradable poly(lactic acid) (PLA) as hydrophobic block and poly(ascorbyl acrylate) (PAAA) as hydrophilic block. When the nanocarriers formed via the self-assembly of the amphiphilic block copolymers poly(lactic acid)-*block*-poly(ascorbyl acrylate) (PLA-*block*-PAAA) have biodegradable hydrophobic compartment for encapsulating anticancer drugs, it is expected that polymeric AA as hydrophilic shell will exhibit exceptional targeting and antitumoral properties. In this work, the fabrication of novel amphiphilic block copolymers PLA-*block*-PAAA was performed by a combination of ring-opening polymerization (ROP) with atom transfer radical polymerization (ATRP), followed by hydrogenation under normal pressure. All of the intermediates and final products were characterized by nuclear magnetic resonance (NMR) and gel permeation chromatography (GPC). Their thermal physical properties and crystallinity were investigated by differential scanning calorimetry (DSC), thermal gravimetric analysis (TGA), and wide angle X-ray diffraction (WAXD). The amphiphilic block copolymers can self-assemble into spherical micelles through the study of dynamic light scattering (DLS) and cryo-transmission electron microscope (cryoTEM).

EXPERIMENTAL

Materials

CuBr purchased from Aldrich was purified by stirring in acetic acid overnight, followed by washing with ethanol and diethyl ether and dried in vacuum. Triethylamine and methylene dichloride (CH₂Cl₂) were dehydrated with KOH and CaCl₂ overnight and distilled, respectively. Toluene and tetrahydrofuran (THF) were dried using sodium with benzophenone as color indicator. All of the above purified solvent and reagents were stored in solvent storage flasks before use. The other reagents such as 2-bromopropionyl bromide, pentamethyldiethylene triamine (PMDTA), and stannous octoate from Aldrich and AA, ethylene glycol, acryloyl chloride, benzyl bromide, and CuBr₂ from Sinopharm Chemical (China) were used as received without further treatment.

Measurements

The ¹H and ¹³C NMR spectra were recorded on a 400 MHz NMR spectrometer (Bruker, Germany) at room temperature using deuterated chloroform (CDCl₃) or deuterated dimethylsulfoxide (DMSO-*d*₆) as solvent. The chemical shifts were measured against the solvent signals of CDCl₃ or DMSO-*d*₆ as internal standard. The molecular weights of the polymers were determined with Waters 515-2410 GPC instrument equipped with Styragel HT6E-HT5-HT3 chromatographic column following a guard column and a differential refractive-index detector. The sample solution was filtered with a 0.45 μm syringe filter before ejection. The measurements were performed using THF as eluent at a flow rate of 1.0 mL min⁻¹ at 30 °C and a series of narrow polystyrene standards for the calibration of the columns. UV-vis spectra were recorded by a Hitachi U-3010 UV-vis spectrometer (Hitachi High-Technologies, Tokyo, Japan). The fluorescence spectra were recorded by a Hitachi F-4500 Fluorescence instrument (Hitachi High-Technologies) at ambience. Fourier transform infrared (FTIR) spectra were measured on a Nicolet 5700 FTIR spectrometer with 32 accumulations at a resolution of 2.0 cm⁻¹ at room temperature for the samples. WAXD patterns of samples were collected on a Shimadzu XRD-6000 diffractometer with Cu Kα radiation (40 kV, 30 mA, λ = 1.5418 Å).

DLS measurements on polymeric micelles were performed using a "Zetaplus" zeta potential analyzer (Brookhaven Instrument) equipped with ZetaPlus Particle Sizing software and with 35-mW solid state laser operated at a laser light wavelength of 660 nm. The size measurements were carried out at 25 °C at a scattering angle of 90°.

The morphological observation of the micelles was carried out on a Hitachi H800 transmission electron microscopy (TEM; Hitachi High-Technologies) operated with 100 kV. For sample preparation, a drop of the filtered sample solution was dropped on a carbon-coated copper grid, excess solution was wicked away with filter paper, and the sample was left dried in air. Samples for cryogenic TEM (cryoTEM) measurement were prepared as follows: nanosized micellar solution was loaded onto holey carbon film-supported grids. Vitrobot (produced by FEI company) was used to make a thin aqueous film blotting with filter paper and the immediate plunging into liquid ethane. The frozen grids were stored in liquid nitrogen and transferred to a cryo-transfer holder under liquid nitrogen at ~ -180 °C. Images were recorded on a CCD camera (2k × 2k, Gatan) using a Tecnai 20 field emission gun electron microscope operated at 120 kV with low-dose mode.

Synthesis of Monomer 6-Acrylate-2,3-*O,O*-dibenzyl-*L*-ascorbic acid

The synthesis procedure of monomer 6-acrylate-2,3-*O,O*-dibenzyl-*L*-ascorbic acid (BnAAA) included two steps. The first step was performed using modified procedure. The mixture of AA (6.0 g, 34.0 mmol), potassium carbonate (11.8 g, 85.0 mmol), and *N,N'*-dimethylformamide (DMF) (20 mL) charged in a 100-mL three-necked round bottom flask was stirred for an hour at 50 °C, followed by the dropwise addition of benzyl bromide (12.0 g, 70 mmol) in DMF (15 mL).

After kept stirring for 5 h, the reaction solution was filtered with celite, and the celite column was rinsed by ethyl acetate. The combined organic phase was washed with distilled water several times, and dried with anhydrous MgSO_4 . The concentrated solution was purified by column chromatograph with ethyl acetate/hexane ($v/v = 1/1$) as eluent to give slight yellow solid product 2,3-*O,O*-dibenzyl-*L*-ascorbic acid (BnAA) in 40% yield (4.8 g).

^1H NMR (400 MHz, CDCl_3) δ (ppm): 7.19–7.38 (m, 10H, $2\text{C}_6\text{H}_5$), 5.03–5.44 (m, 4H, $2\text{CH}_2\text{Ph}$), 4.67 (d, $J = 4.0$ Hz, 1H, hydrogen on C-4), 3.94 (br, 1H, hydrogen on C-5), 3.73–3.78 (m, 2H, hydrogen on C-6), 3.39 (br, 1H, OH on C-5), 3.14 (br, 1H, OH on C-6). ^{13}C NMR (100 MHz, CDCl_3) δ (ppm): 170.2, 157.8, 135.9, 135.3, 129.1, 128.7, 127.8, 121.1, 76.1, 74.1, 73.6, 69.9, 63.4. FTIR (KBr disk): ν_{OH} , 3425 cm^{-1} (s), $\nu_{\text{C-H}}$, 2923 cm^{-1} (m), 2852 cm^{-1} (s), 1744 cm^{-1} (m), $\nu_{\text{C=C}}$, 1655 cm^{-1} (s).

For the second step, BnAAA preparation was conducted by the reaction of BnAA (4.8 g, 13.5 mmol), acryloyl chloride (1.5 g, 16.2 mmol) and triethylamine (1.8 g, 17.5 mmol) in anhydrous CH_2Cl_2 (20 mL) at 0 °C for 5 h. The reaction solution was filtered, and the filtrate was washed by distilled water three times. The concentrated organic mixture was purified by column chromatograph with the mixture of ethyl acetate and hexane ($v/v = 2/5$) as eluent to obtain white solid product in 54% yield (3.0 g).

^1H NMR (400 MHz, CDCl_3) δ (ppm): 7.20–7.34 (m, 10H, $2\text{C}_6\text{H}_5$), 6.43 (d, $J = 12.0$ Hz, 1H, $\text{CH}_2=\text{CH}$), 6.14 (q, $J = 12.0$ Hz, 1H, $\text{CH}_2=\text{CH}$), 5.85 (d, $J = 12.0$ Hz, 1H, $\text{CH}_2=\text{CH}$), 5.17 (dd, $J = 12.0$ Hz, 4H, 2PhCH_2), 4.69 (d, $J = 2.0$ Hz, 1H, hydrogen on C-4 of AA), 4.28–4.42 (m, 2H, hydrogen on C-6 of AA), 4.10–4.15 (m, 1H, hydrogen on C-5 of AA), 2.99 (br, 1H, OH linking with C-5 of AA). ^{13}C NMR (100 MHz, CDCl_3) δ (ppm): 169.7, 166.0, 157.0, 136.0, 135.4, 131.9, 129.2, 128.8, 127.9, 121.4, 75.7, 74.1, 73.8, 67.9, 64.9. IR (KBr disk, cm^{-1}): ν_{OH} , 3440 cm^{-1} (s), $\nu_{\text{C-H}}$, 2956 cm^{-1} (s), 2923 cm^{-1} (vs), 2852 cm^{-1} (s), $\nu_{\text{C=O}}$, 1764 cm^{-1} (s) and 1728 cm^{-1} (s). Calcd. for $\text{C}_{23}\text{H}_{22}\text{O}_7$: C, 67.31; H, 5.40%. Found: C, 67.32; H, 5.50%.

Synthesis of Initiator HEBP

In a 100-mL three-necked flask containing ethylene glycol (16.6 g, 26.7 mmol) and triethylamine (2.8 g, 26.7 mmol) in THF (40 mL), 2-bromopropionyl bromide (5.8 g, 26.7 mmol) in THF (10 mL) was stepwisely added and kept stirring at 0 °C for 6 h. After filtration, the filtrate was sequentially washed with 0.01 mol L^{-1} HCl, 0.01 mol L^{-1} NaOH, and distilled water. The combined organic phase was dried over anhydrous MgSO_4 and concentrated. The crude product was further purified by column chromatograph with the mixture of ethyl acetate and hexane ($v/v = 1/3$) as eluent to obtain yellow liquid product in 63% yield (3.32 g).

^1H NMR (400 MHz, CDCl_3) δ (ppm): 4.45 (q, $J = 8.0$ Hz, 1H, CH_3CHBr), 4.31 (m, 2H, CH_2OCO), 3.85 (t, $J = 4.0$ Hz, 2H, $\text{HOCH}_2\text{CH}_2\text{OCO}$), 2.03 (br, 1H, OH), 1.83 (d, $J = 4.0$ Hz, 3H, CH_3CHBr). ^{13}C NMR (100 MHz, CDCl_3) δ (ppm): 170.5, 67.2, 60.6, 39.9, 21.5. FTIR (KBr disk): ν_{OH} , 3434 cm^{-1} (s), $\nu_{\text{C-H}}$, 2954 cm^{-1} (m), 2923 cm^{-1} (m), $\nu_{\text{C=O}}$, 1736 cm^{-1} (s).

Synthesis of Poly(lactic acid) via ROP

In a typical ROP procedure, a Schlenk flask degassed by three vacuum-nitrogen cycles was charged with $\text{Sn}(\text{Oct})_2$ (56.3 mg, 0.14 mmol), initiator 2-hydroxyethyl- α -bromopropionate (HEBP; 54.7 mg, 0.28 mmol), *L*-lactide (2.0 g, 13.9 mmol), and toluene (4.0 mL). The reaction equipment was immersed in an oil bath thermostated at 70 °C. After predetermined polymerization time, the reaction solution was precipitated in the cold methanol (200 mL) for three times. The polymers were dried in vacuum at room temperature for 5 h.

^1H NMR (400 MHz, CDCl_3) δ (ppm): 5.15 (m, nH, CH in the repeating unit), 4.34–4.37 (m, 6H, CH_3CHBr , $\text{CO}_2\text{CH}_2\text{CH}_2\text{OCO}$ and CH_3CHOH), 1.81 (d, $J = 4.0$ Hz, 3H, CH_3CHBr), 1.57 (d, $J = 8.0$ Hz, nH, CH_3 in the repeating unit). ^{13}C NMR (100 MHz, CDCl_3) δ (ppm): 169.7, 69.1, 66.7, 63.1, 62.6, 39.4, 21.4, 20.4, 16.8. FTIR (KBr disk): $\nu_{\text{C-H}}$, 2955 cm^{-1} (s), 2924 cm^{-1} (vs), 2852 cm^{-1} (s), $\nu_{\text{C=O}}$, 1757 cm^{-1} (s).

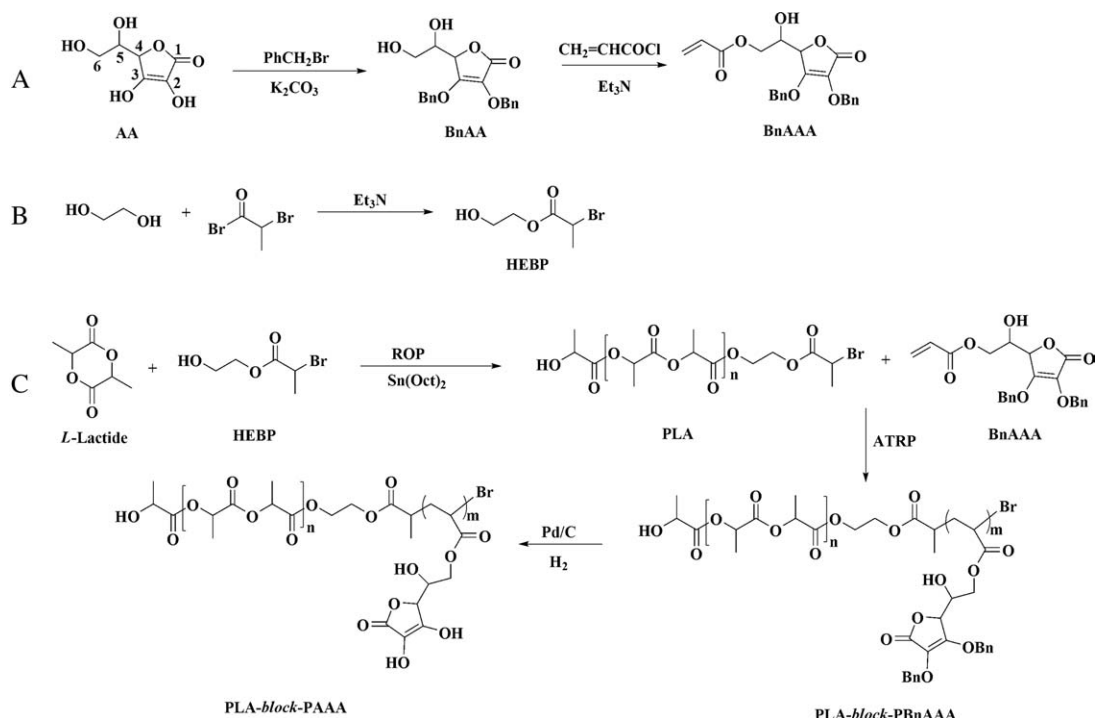
Synthesis of Block Polymers PLA-block-PBnAAA via ATRP

Typically, a Schlenk flask with a magnetic stir bar was charged with CuBr (10.0 mg, 0.068 mmol), macroinitiator PLA-Br (396.0 mg, 0.068 mmol) and CuBr_2 (0.8 mg, 0.0034 mmol). The flask was degassed by three vacuum-nitrogen cycles, and the liquid materials including ligand PMDETA (14.2 mg, 0.082 mmol), monomer BnAAA (0.7 g, 1.71 mmol) and toluene (3.0 mL), which were degassed by nitrogen bubbling for 20 min before use, were introduced into the reaction flask using syringes under nitrogen atmosphere. The reaction equipment was further degassed by three freeze-pump-thaw cycles, and then immersed in a thermostated oil bath. After predetermined polymerization time, the cooled down reaction solution was precipitated in cold methanol (150 mL) three times, and the solid was dried in vacuum at ambience for 6 h in 41% yield (0.45 g).

^1H NMR (400 MHz, CDCl_3) δ (ppm): for PLA block, 5.13–5.29 (m, nH, CH), 1.58 (s, 3nH, CH_3); for PBnAAA block, 7.10–7.40 [m, 10mH (m representing repeating unit number of PBnAAA block), $2\text{C}_6\text{H}_5$], 4.98 (m, 4mH, 2PhCH_2), 4.58 (m, mH, hydrogen on C-4 of AA), 4.07–4.38 (m, 3mH, hydrogen on C-5 and C-6 of AA), 2.45 (m, mH, CH on the backbone), 1.75–1.97 (m, 2mH, CH_2 on the backbone). ^{13}C NMR (100 MHz, CDCl_3) δ (ppm): 175.1, 169.7, 157.3, 136.2, 137.2, 129.0, 128.7, 127.9, 121.5, 76.3, 74.2, 73.6, 69.1, 66.8, 41.2, 37.7, 20.6, 16.8. FTIR (KBr disk): $\nu_{\text{C-H}}$, 2955 cm^{-1} (m), 2923 cm^{-1} (m), $\nu_{\text{C=O}}$, 1755 cm^{-1} (s).

Synthesis of Amphiphilic Block Copolymer PLA-block-PAAA via Hydrogenation Under Normal Pressure

Palladium on carbon (10%, 63 mg) as catalyst was added into the polymer solution comprised of poly(lactic acid)-block-poly(benzyl ascorbyl acrylate) (PLA-block-PBnAAA; 630 mg), anhydrous THF (20 mL) and methanol (15 mL). The benzyl deprotection was performed under normal H_2 pressure at 30 °C for overnight, and then Pd/C catalyst was filtered off and washed with methanol. After complete evaporation of the combined filtrate, the solid was redissolved in a small amount of THF and precipitated in cold ether (50 mL) to obtain gray white solid in 63% yield (400 mg).



SCHEME 1 Synthesis pathway of monomer (A), initiator HEBP (B), and block polymers (C).

¹H NMR (400 MHz, DMSO-*d*₆) δ (ppm): for PLA block, 5.19 (m, nH, CH), 1.45 (s, 3nH, CH₃); for PAAA block, 4.64 (m, mH, hydrogen on C-4 of AA), 4.04–4.21 (m, 3mH, hydrogen on C-5 and C-6 of AA), the main chain signals of PAAA block were covered by DMSO-*d*₆. FTIR (KBr disk): ν_{OH} , 3438 cm⁻¹ (s), $\nu_{\text{C-H}}$, 2955 cm⁻¹ (m), 2924 cm⁻¹ (m), $\nu_{\text{C=O}}$, 1758 cm⁻¹ (s).

Characterization of Thermal Physical Properties

DSC experiments were conducted on a Mettler Toledo. The polymer sample (8.0–10.0 mg) encapsulated in an aluminum pan was run at a scanning rate of 20 °C min⁻¹ over a temperature range of 25–190 °C with ultra pure nitrogen as purge gas. Melting points (T_m) were evaluated using the top temperatures of the corresponding main peak. Thermogravimetric analysis (TGA) was used on a Mettler Toledo TGA, and the prepared copolymer (4.0–5.0 mg) was scanned at 10 °C min⁻¹ from 30 to 700 °C under nitrogen atmosphere at a flowing rate of 50 mL min⁻¹. Peak top temperature (T_d s) occurring in the differentiated TGA (dTGA) traces was used to assess thermal degradation behavior and stabilities for the synthesized polymers.

Critical Micelle Concentration

Critical micelle concentration (CMC) of the amphiphilic block copolymer was determined by steady-state fluorescence spectrometry with pyrene as a fluorescent probe. The concentration of block polymer was varied from 1.0×10^{-5} to 2.0 mg mL⁻¹, and the concentration of pyrene was fixed at 1.73×10^{-3} μ M. The fluorescence spectra were recorded using Hitachi F-4500 Fluorescence spectrometer with the emission wavelength of 395 nm, and the excitation fluorescence was monitored at 338 and 333 nm. CMC was esti-

mated as the cross-point when extrapolating the intensity ratio I_{338}/I_{333} at low- and high-concentration regions.

Turbidity Measurement and Micelle Formation

Turbidity measurements were performed according to the published procedures.²¹ Deionized water was added at a rate of 5 μ L min⁻¹ to the polymer in dioxane or DMSO (0.5 wt %, 2 mL) under slight shaking. After each addition of water, the solution was left to equilibrate for a while until the optical intensity was stable. The optical intensity (turbidity) was measured at a wavelength of 600 nm using a quartz cell (path length: 1 cm) with Hitachi U-3010 UV-vis spectrometer. The cycle of water addition, equilibrium, and measurement was continued until the desired amount of water was achieved (50–70 wt %). The micelle solution was obtained by dialyzing the mixture against deionized water (500 mL) for 2 days during which the water was refreshed every 4 h.

RESULTS AND DISCUSSION

Synthesis and Characterization of PLA-block-PAAA

Among a variety of the reported polymerization methodologies, ATRP and ROP are two disparate polymerization techniques. ATRP is available to acrylate-series monomers, and ROP favors for lactone monomers polymerization. A combination of ATRP and ROP is one efficient strategy to fabricate various materials.^{22–26} As outlined in Scheme 1(C), the synthesis route of PLA-block-PAAA comprises of ROP, ATRP, and hydrogenation. The initiator HEBP is one key to perform the combination of ATRP and ROP, and it is also a bridge to link PLA and PAAA blocks in the resulting polymers. Based on the preparation of HEBP by the reaction of 2-

bromopropionyl bromide with ethylene glycol [Scheme 1(b)], homopolymers PLA with different molecular weights were carried out in the presence of stannous octoate via ROP, and the polymerization results are summarized in Supporting Information Table S1. Subsequently, PLA bearing 2-bromopropionyl group initiated the polymerization of monomer BnAAA (its preparation route is depicted in Scheme 1(A)) via ATRP to fabricate a series of diblock copolymers PLA-*block*-PBnAAA.

The chemical structures of homopolymer PLA and block copolymer PLA-*block*-PBnAAA were evidenced by ^1H NMR techniques, and the typical ^1H NMR spectra are depicted in Figure 1. For homopolymer PLA, the proton signals of methine and methyl on the repeating unit appeared at 5.16 and 1.57 ppm, respectively, and the proton peaks from the initiation moiety [as marked c, d, and e in Fig. 1(A)] were overlapped ~ 4.37 ppm. It is noteworthy that degree of polymerization (DP) for lactide listed in Supporting Information Table S1 was calculated by comparing the integrals at 5.16 and 1.81 ppm associated with methyl peak (f) in the initiation segment. For PLA-*block*-PBnAAA, besides the signals of PLA block appearing at corresponding chemical shift, the proton (i, h, g) signals on C-4, C-5, and C-6 [marked in Scheme 1(A)] of AA moiety were found at 4.56, 4.25, and 4.06 ppm [Fig. 1(B)], respectively. The peaks at 4.97 and 7.18–7.30 ppm were attributed to the respective methylene (j) and phenyl ring (k, l, m) of benzyl group in the PBnAAA block. The methine (f) and methylene (e) protons on PBnAAA backbone were present at 2.42 and 2.00 ppm. Based on the aforementioned DP of PLA block calculated from ^1H NMR results, DP of PBnAAA block was estimated by comparing the integrals at 5.16 and 4.56 ppm, as summarized in Table 1. Additionally, GPC analysis for the block polymers PLA-*block*-PBnAAA revealed unimodal and narrow distribution (1.25–1.39) without macroinitiator PLA (Fig. 2), which further substantiated the successful synthesis of structurally well-defined block copolymers PLA-*block*-PBnAAA.

The hydrogenation to remove benzyl group was performed using Pd/C as catalyst under normal pressure at room temperature. One representative ^1H NMR spectrum of PLA-*block*-PAAA is shown in Figure 1(c), in which the peaks associated with PLA block ($\delta = 5.16$ and 1.57 ppm) and AA units ($\delta = 4.63$, 4.05 and 4.19 ppm) were obviously observed. It is of great importance that the signals at 7.28 and 4.95 ppm assigned to phenyl ring and methylene of benzyl group almost completely disappeared, indicating that the hydroxyl groups at 2 and 3 positions of AA skeleton were successfully set free. Because of the presence of deuterated DMSO's signal, the methine signals of PAAA backbone were hidden at 2.42 ppm. Depending on the ratio change of the integrals for the phenyl ring ($\delta = 7.28$ ppm) and methine of PLA block ($\delta = 5.16$ ppm) before and after hydrogenation, the measured hydrogenation efficiency is over 90% for these amphiphilic block copolymers. The ratio of PLA to PAAA block estimated by comparing the integrals at 5.16 to 4.63 ppm is close to the composition ratio of the copolymers before hydrogenation, as tabulated in Table 1. Chloroform is a good solvent for PLA-*block*-PBnAAA, whereas the hydrogenation

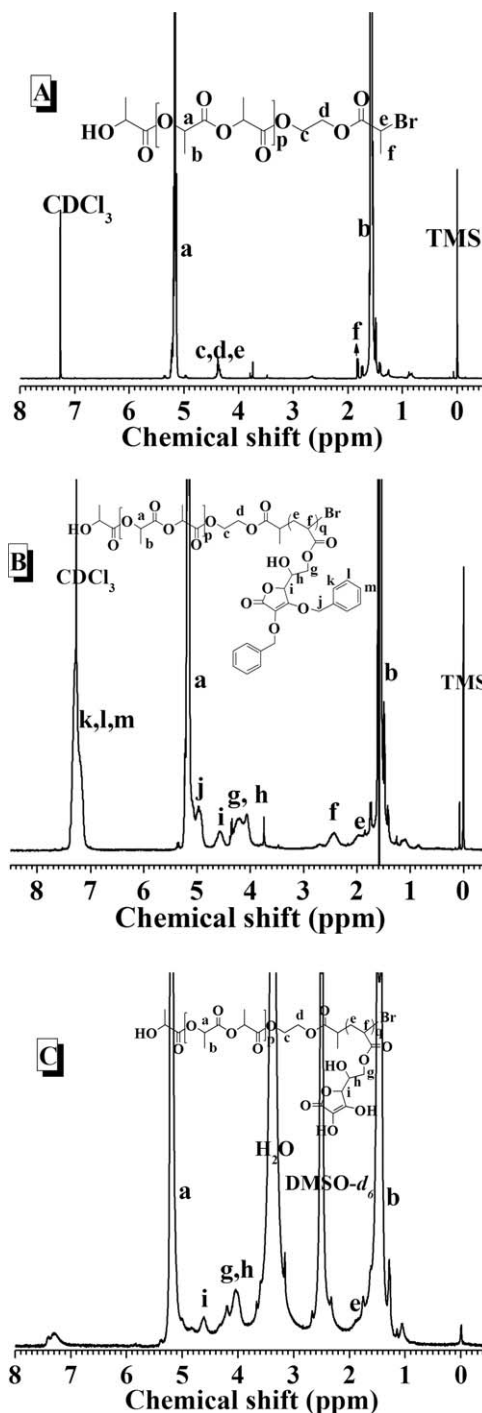


FIGURE 1 (A) ^1H NMR spectrum of homopolymer PLA-3. (B) ^1H NMR spectrum of PLA-*block*-PBnAAA (63/10). (C) ^1H NMR spectrum of PLA-*block*-PAAA (63/10).

resultants PLA-*block*-PAAA can selectively dissolve in strong polar solvent such as DMSO or DMF. The solubility changing before and after hydrogenation indirectly supported the generation of amphiphilic block copolymers.

Thermal Physical Properties of PLA-*block*-PAAA

The thermal stability of the amphiphilic copolymers PLA-*block*-PAAA was evaluated using TGA. Figure 3(A) shows the

TABLE 1 Molecular Characteristics of Block Copolymers PLA-*block*-PBnAAA and PLA-*block*-PAAA

MI ^a	DP of MI	Molar ratio of MI and Monomer	Temp. (°C)	Time (h)	DP _{ratio} ^b (NMR)	PLA- <i>block</i> -PBnAAA			PLA- <i>block</i> -PAAA	
						M _n ^c (NMR)	M _n ^d (GPC)	M _w /M _n ^e (GPC)	Hydrogenation Efficiency (%) ^f	DP _{ratio} ^g (NMR) ^g
PLA-1	40	1/25	80	15	40/5	7,800	9,700	1.25	90	40/5
PLA-2	44	1/40	70	40	44/10	10,400	10,900	1.39	90	44/9
PLA-3	63	1/40	70	40	63/7	11,900	13,300	1.26	99	63/7
PLA-3	63	1/40	80	40	63/10	13,100	13,500	1.34	97	63/10

^a PLA as macroinitiator was tabulated in Supporting Information Table S1 in detailed.

^b DP_{ratio} represented polymerization degree ratio of PLA block to PBnAAA block measured by ¹H NMR.

^c M_n(NMR) represented molecular weight calculated by ¹H NMR results.

^d M_n(GPC) indicated molecular weight determined by GPC measurement.

^e Obtained by GPC.

^f Calculated by ¹H NMR results.

^g DP_{ratio} represented polymerization degree ratio of PLA block to PAAA block measured by ¹H NMR.

weight-loss curves for a series of amphiphilic copolymers compared with homopolymers PLA and PAAA, and the peak top temperature (T_d s) occurring in the differentiated TGA traces was used to quantitatively assess thermal degradation behavior. For homopolymer PLA, no obvious weight loss happened before 200 °C and its rapid thermal degradation occurred at ~257 °C. Interestingly, the degradation behavior of homopolymer PAAA ($M_n = 9200$ and $M_w/M_n = 1.18$) was exhibited three stages in the course of measurement [the inset of Fig. 3(A)]. Moreover, when PAAA was heated to 700 °C, nearly 40% of the initial weight remained. For the synthesized copolymers PLA-*block*-PAAA, their T_d s between 300 and 340 °C were 50–80 °C higher than homopolymer PLA, indicating that PAAA introduction is capable of improving the thermal stability for the overall copolymer. Except the copolymer PLA-*block*-PAAA (44/9) (44 and 9 stand for DP of lactide and ascorbyl acrylate) showing stepwise two-step thermal degradation, the other copolymers showed only one-step degradation profiles. For the copolymers PLA-*block*-PAAA (63/7) and PLA-*block*-PAAA (63/10) with identical PLA length, PLA-*block*-PAAA (63/10) having long PAAA block presented slightly higher thermal stability (T_d value is ~331 °C). For these four block polymers, more than 20% of overall weights still remained above 500 °C, which was probably the result of the incomplete degradation of PAAA part and residual Pd/C.

The melting behavior of the amphiphilic block copolymers was investigated by DSC, and the heating scans were exhibited in Figure 3(B). Homopolymer PLA-3 had one T_m at 145 °C and one T_g around 66 °C which are similar to those reported previously,²⁷ whereas homopolymer PAAA ($M_n = 9200$ and $M_w/M_n = 1.18$) did not show obvious T_m . For block copolymers PLA-*block*-PAAA, they only exhibited T_m and T_g of PLA block, among which T_m of PLA block was lower than the corresponding homopolymer, possibly because of the presence of PAAA blocks confining the melting behavior of PLA segment. For PLA-*block*-PAAA (44/9) and PLA-*block*-PAAA (63/7), one endothermic peak appeared between 60 and 80 °C covering T_g of PLA block, and the reason accounting for the peak remained unclear so far. The

crystalline behavior of PLA-*block*-PAAA was measured by WAXD, which was in agreement with DSC results. As shown in Figure 3(C), homopolymer PAAA presented obvious

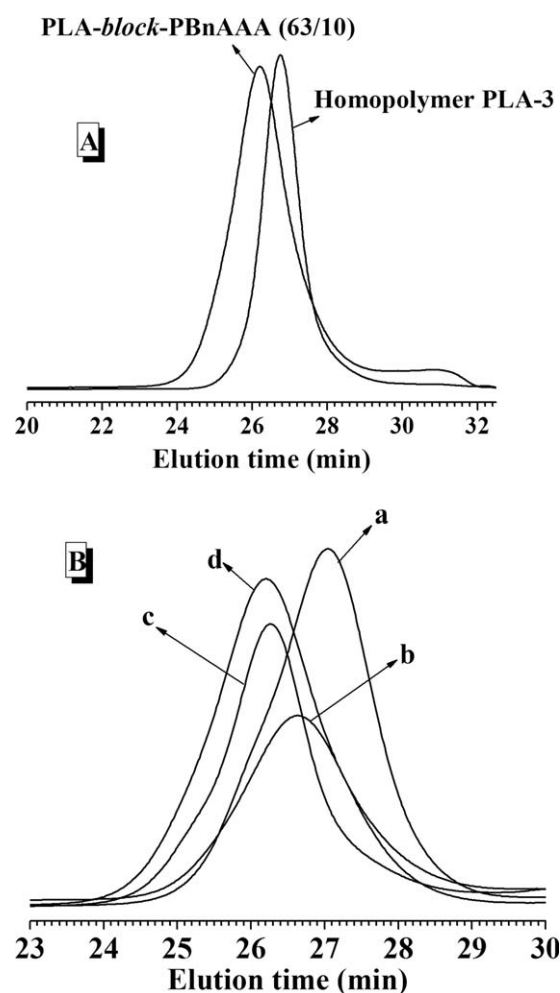


FIGURE 2 (A) GPC traces of PLA-3 and PLA-*block*-PBnAAA (63/10). (B) GPC traces of PLA-*block*-PBnAAA (40/5, a), (44/10, b), (63/7, c), and (63/10, d).

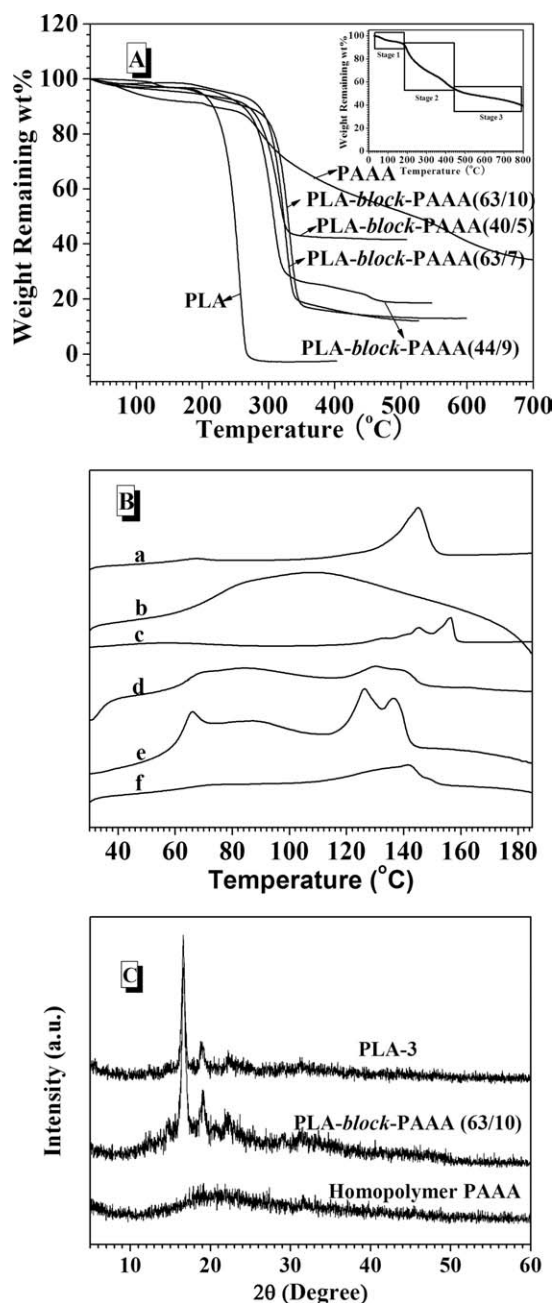


FIGURE 3 (A) TGA curves of homopolymers PLA, PAAA, and block copolymers PLA-*block*-PAAA. (B) DSC heating curves of PLA (a), PAAA (b), PLA-*block*-PAAA (40/5, c), PLA-*block*-PAAA (44/9, d), PLA-*block*-PAAA (63/7, e), and PLA-*block*-PAAA (63/10, f). (C) WAXD patterns of PLA, PAAA, and PLA-*block*-PAAA (63/10) at 25 °C.

amorphous phase, and PLA-*block*-PAAA (63/10) have only two crystalline peaks appearing at $2\theta = 16.6^\circ$ and 19.0° , corresponding to (200)/(110) and (203) reflections of PLA block, respectively.²⁸ Other block copolymers had identical WAXD results (not shown).

Self-Assembly of Amphiphilic Block Copolymers PLA-*block*-PAAA in Aqueous Solution

The amphiphilicity of the copolymers PLA-*block*-PAAA provides one good possibility to form assembly aggregates in

aqueous solution. CMC determination was carried out for these copolymers by the use of fluorescence probe technique.^{29–32} The characteristic shift of pyrene excitation spectra from 333 to 338 nm indicating pyrene partition into the hydrophobic core of the micelle was utilized to determine the CMC of the block copolymers in aqueous solution. Figure 4(A) shows the intensity ratio of I_{338}/I_{333} in the pyrene excitation spectra as a function of the logarithm of the copolymer concentrations. A negligible change in the intensity ratio of I_{338}/I_{333} was detected at the low-concentration range, whereas the intensity ratio exhibited a substantial increase with the copolymer concentration increasing, indicating that the pyrene molecules incorporated into the hydrophobic region. The I_{338}/I_{333} versus $\log C$ plot presented one sigmoid curve; therefore, the CMC value was determined from the cross-over point in the low-concentration range. The CMCs of the copolymers ranged between 13 and 28 mg L⁻¹ in Table 2. Moreover, for these amphiphilic polymers having

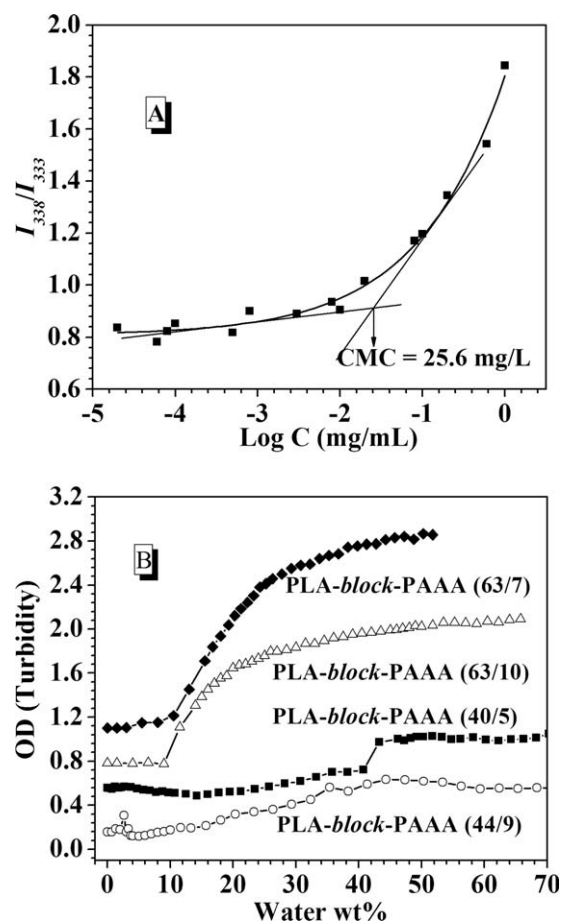


FIGURE 4 (A) Plots of I_{338}/I_{333} ratio of pyrene excitation spectra in water as a function of PLA-*block*-PAAA (44/9) concentration at 25 °C. (B) Turbidity (optical density) curves of the amphiphilic polymers solution as a function of the amount of deionized water added to the polymer solution. The turbidity values for water addition lower than 10 wt % are close to zero. The curves of PLA-*block*-PAAA (40/5), (63/10), and (63/7) are shifted for clarity.

TABLE 2 Solution Properties of Polymeric Micelles Formed From PLA-*block*-PAAAs

Amphiphilic Copolymers	CMC ^a (mg/L)	DLS	
		Mean Diameter (nm) ^b	PDI ^c
PLA- <i>block</i> -PAAA(40/5)	13.4	180.9	0.148
PLA- <i>block</i> -PAAA(44/9)	25.6	135.6	0.209
PLA- <i>block</i> -PAAA(63/7)	21.1	216.5	0.171
PLA- <i>block</i> -PAAA(63/10)	27.2	42.2	0.157

^a Measured at 25 °C.

^b The particle average dimension determined by DLS at 25 °C.

^c PDI meant polydispersity index of particle dimension measured by DLS.

identical PLA block length, the effect of shorter hydrophilic block is evident in the lower CMC value, indicating a greater driving force for the self-assembly in aqueous solution.

Dioxane and DMSO are good nonselective solvents for PLA and PAAA, whereas water is a good selective solvent for PAAA but is poor for PLA. Therefore, the addition of water into the amphiphilic copolymers in dioxane would induce the self-assembly of amphiphilic polymer PLA-*block*-PAAA.²¹ On the progressive addition of water into the corresponding polymer solution at the concentration of 0.5 wt %, the turbidity diagrams of the copolymers PLA-*block*-PAAA were obtained using UV-vis spectrometer. As shown in Figure 4(B), the turbidity curves exhibited one jump on the gradual addition of water, followed by the turbidity values reaching a plateau, which is probably associated with the formation of the nanoscaled aggregates. The polymers having long PLA blocks, such as PLA-*block*-PAAA (63/7) and (63/10), showed relatively fast and obvious jump when water content reached 10% of the whole mixture, whereas the polymers bearing short PLA blocks did not exhibit certain nanoaggregation behavior until water content was over 40%. These results further suggest the amphiphilic polymers bearing long hydrophobic block have stronger driving force of self-assembly in aqueous solution. The final turbid mixtures were transferred into the dialysis bag (cut-off molecular weight 3500) and extensively dialyzed against deionized water for complete removal of organic solvent. The morphology and size distributions of the copolymer aggregates were investigated by TEM observation and DLS, respectively.

All of the samples were not filtered before TEM and DLS measurements so that the pristine state of the dissolved copolymer was analyzed in this study. The morphology of the polymeric aggregates was examined by cryoTEM. Figure 5(A) presents one representative cryoTEM pattern for the copolymer PLA-*block*-PAAA (63/7), in which the aggregates exhibited the closely spherical polymeric micelles with diameter range of 100–150 nm. The micellar size of PLA-*block*-PAAA (63/7) was further determined by DLS [Fig. 5(B)]. These polymeric micelles had characteristic bimodal distributions with a small size component around 120 nm and a large

size component about 300 nm, and their mean hydrodynamic diameters were ~216 nm (Table 2). In theory, the contour length of the polymer PLA-*block*-PAAA (63/7) is calculated to be ~32 nm, with the PLA segment estimated to be ~30 nm and the PAAA moiety estimated to be ~1.8 nm (it is assumed that carbon-carbon single bond length is about 1.54 Å, and carbon-oxygen single bond length is ~1.40 Å). However, the mean particle size in the DLS measurement is much larger than that calculated, indicating that the observed spherical nanoparticles are probably micellar aggregates.^{33,34} The similar observations were performed as shown in Supporting Information Figures S5 and S6. The micellar sizes in the majority for all of these polymers are below 150 nm, particularly for PLA-*block*-PAAA (44/9) and PLA-*block*-PAAA (63/10), which have potential to increase the accumulation possibility of these nanocarriers at pathological sites.³⁵

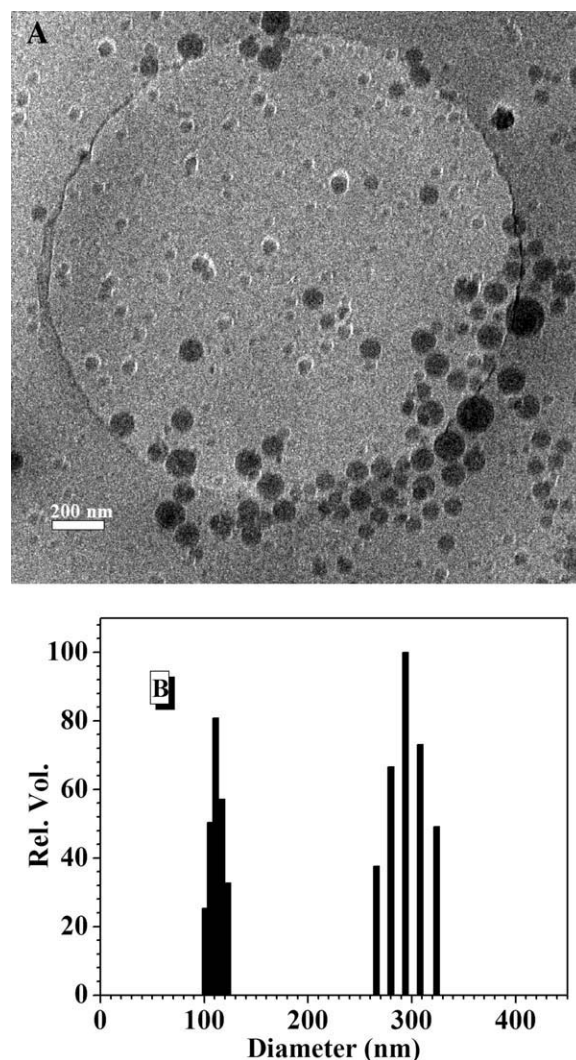


FIGURE 5 (A) CryoTEM image of PLA-*block*-PAAA (63/7). (B) DLS graph for micellar size distribution of PLA-*block*-PAAA (63/7).

CONCLUSIONS

Based on the reported special physiological function of AA and combined with drug delivery nanotechnology, one type of polymeric micelles formed from the amphiphilic block copolymers PLA-*block*-PAAA with biodegradable PLA as hydrophobic block and potential targeting PAAA as hydrophilic block was explored for the first time. The synthesis of PLA-*block*-PAAA was conducted via the three steps including ROP of lactide, ATRP of BnAAA, and hydrogenation with Pd/C as catalyst under normal pressure. The CMC values of the copolymers measured by fluorescence probe techniques were in the range of 13 and 28 mg L⁻¹. These amphiphilic polymers self-assembled to form spherical micellar aggregates with average size in the range of 40–220 nm, which is suitable to the circulation *in vivo*. This study explored the possibility of polymeric AA as hydrophilic block in the amphiphilic copolymers, and this class of nanocarriers could be used as a selective drug delivery to facilitate the potential therapeutic for the treatment of some brain-associated diseases and tumor cure. Further investigation on their biocompatibility and targetability is underway in our laboratory.

This work was supported by National Natural Science Foundation of China (NSFC, Grant No. 20804003), Scientific Research Foundation for the Returned Overseas Chinese Scholars, State Education Ministry, and Chinese Universities Scientific Fund.

REFERENCES AND NOTES

- 1 Torchilin, V. P. *Pharm Res* 2007, 24, 1–16.
- 2 Marcato, P. D.; Durán, N. *J Nanosci Nanotechnol* 2008, 8, 2216–2229.
- 3 Nair, L. S.; Laurencin, C. T. *Prog Polym Sci* 2006, 32, 762–798.
- 4 Mundargi, R. C.; Babu, V. R.; Rangaswamy, V.; Patel, P.; Aminabhavi, T. M. *J Control Release* 2008, 125, 193–209.
- 5 Kabanov, A. V.; Gendelman, H. E. *Prog Polym Sci* 2007, 32, 1054–1082.
- 6 Bergley, D. J. *J Pharm Pharmacol* 1996, 48, 136–146.
- 7 Spector, R. *Pharmacology* 2000, 60, 58–73.
- 8 Chen, Q.; Espey, M. G.; Krishna, M. C.; Mitchell, J. B.; Corpe, C. P.; Buettner, G. R.; Shacter, E.; Levine, M. *Proc Natl Acad Sci USA* 2005, 102, 13604–13609.
- 9 Chen, Q.; Espey, M. G.; Sun, A. Y.; Lee, J. H.; Krishna, M. C.; Shacter, E.; Choyke, P. L.; Pooput, C.; Kirk, K. L.; Buettner, G. R.; Levine, M. *Proc Natl Acad Sci USA* 2007, 104, 8749–8754.
- 10 Agus, D. B.; Vera, J. C.; Golde, D. W. *Cancer Res* 1999, 59, 4555–4558.
- 11 Tsukaguchi, H.; Tokui, T.; Mackenzie, B.; Berger, U. V.; Chen, X. Z.; Wang, Y.; Brubaker, R. F.; Hediger, M. A. *Nature* 1999, 399, 70–75.
- 12 Cioffi, N.; Losito, I.; Terzano, R.; Zambonin, C. G. *Analyst* 2000, 125, 2244–2248.
- 13 Manfredini, S.; Pavan, B.; Vertuani, S.; Scaglianti, M.; Compagnone, D.; Biondi, C.; Scatturin, A.; Tanganelli, S.; Ferraro, L.; Prasad, P.; Dalpiaz, A. *J Med Chem* 2002, 45, 559–562.
- 14 Manfredini, S.; Vertuani, S.; Pavan, B.; Vitali, F.; Scaglianti, M.; Bortolotti, F.; Biondi, C.; Scatturin, A.; Prasad, P.; Dalpiaz, A. *Bioorgan Med Chem* 2004, 12, 5453–5463.
- 15 Dalpiaz, A.; Pavan, B.; Vertuani, S.; Vitali, F.; Scaglianti, M.; Bortolotti, F.; Biondi, C.; Scatturin, A.; Tanganelli, S.; Ferraro, L.; Marzola, G.; Prasad, P.; Manfredini, S. *Eur J Pharm Sci* 2005, 24, 259–269.
- 16 D'Souza, G. G. M.; Wang, T.; Rockwell, K.; Torchilin, V. P. *Pharm Res* 2008, 25, 2567–2572.
- 17 Sawant, R. R.; Vaze, O.; D'Souza, G. G. M.; Rockwell, K.; Torchilin, V. P. *Pharm Res* 2011, 28, 301–308.
- 18 Sawant, R. R.; Vaze, O. S.; Rockwell, K.; Torchilin, V. P. *Eur J Pharm Biopharm* 2010, 75, 321–326.
- 19 Salmaso, S.; Pappalardo, J. S.; Sawant, R. R.; Musacchio, T.; Rockwell, K.; Caliceti, P.; Torchilin, V. P. *Bioconjugate Chem* 2009, 20, 2348–2355.
- 20 Martins, D.; Frungillo, L.; Anazzetti, M. C.; Melo, P. S.; Durán, N. *Int J Nanomed* 2010, 5, 77–85.
- 21 Zhang, L. F.; Yu, K.; Eisenberg, A. *Science* 1996, 272, 1777–1779.
- 22 Kataoka, K.; Harada, A.; Nagasaki, Y. *Adv Drug Deliv Rev* 2001, 47, 113–131.
- 23 Lavasanifar, A.; Samuel, J.; Kwon, G. S. *Adv Drug Deliv Rev* 2002, 54, 169–190.
- 24 Rapoport, N. *Prog Polym Sci* 2007, 32, 962–990.
- 25 Gil, E. S.; Hudson, S. M. *Prog Polym Sci* 2004, 29, 1173–1222.
- 26 Soppimath, K. S.; Aminabhavi, T. M.; Kulkarni, A. R.; Rudzinski, W. E. *J Control Release* 2001, 70, 1–20.
- 27 Ueda, A. S.; Chatani, Y.; Tadokoro, H. *Polym J* 1971, 2, 387–397.
- 28 Xiao, H. W.; Lu, W.; Yeh, J. T. *J Appl Polym Sci* 2009, 112, 3754–3763.
- 29 Astafieva, I.; Zhong, X. F.; Eisenberg, A. *Macromolecules* 1993, 26, 7339–7352.
- 30 Wilhelm, M.; Zhao, C. L.; Wang, Y. C.; Xu, R. L.; Winnik, M. A.; Mura, J. L.; Riess, G.; Groucher, M. D. *Macromolecules* 1991, 24, 1033–1040.
- 31 Kalyanasundaram, K.; Thomas, J. K. *J Am Chem Soc* 1977, 99, 2039–2044.
- 32 Chang, Y. K.; Bender, J. D.; Phelps, M. V. B.; Allcock, H. R. *Biomacromolecules* 2002, 3, 1364–1369.
- 33 La, S. B.; Okano, T.; Kataoka, K. *J Pharm Sci* 1996, 85, 85–90.
- 34 Allen, C.; Yu, Y. S.; Maysinger, D.; Eisenberg, A. *Bioconjugate Chem* 1998, 9, 564–572.
- 35 Kwon, G. S.; Okano, T. *Adv Drug Deliv Rev* 1996, 21, 101–106.